The Pion Single-Event Effect Resonance and Its Impact in an Accelerator Environment

Andrea Coronetti, Rubén García Alía, Matteo Cecchetto, Wojtek Hajdas, Daniel Söderström, Arto Javanainen, and Frédéric Saigné

***Abstract*— The pion resonance in the nuclear reaction cross section is seen to have a direct impact on the single-event effect (SEE) cross section of modern electronic devices. This was experimentally observed for single-event upsets and single-event latchup. Rectangular parallelepiped (RPP) models built to fit proton data confirm the existence of the pion SEE cross-section resonance. The impact on current radiation hardness assurance (RHA) soft error rate (SER) predictions is, however, minimal for the accelerator environment since this is dominated by high neutron fluxes. The resonance is not seen to have a major impact on the high-energy hadron equivalence approximation established for testing in mixed-field facilities.**

***Index Terms*— Accelerator, cross section, FLUKA, neutrons, pions, protons, radiation hardness assurance (RHA), single-event effect (SEE), soft error rate (SER).**

I. Introduction

ALIKE protons and neutrons, pions can interact with silicon nuclei by inelastic collisions. The consequent indirect energy deposition along the recoil ionization track can lead to single-event effects (SEEs) in electronic devices. The pion soft error rate (SER) is expected to be similar or higher than those from proton and neutron indirect energy depositions. The potentially higher SER from pions is due to the resonance in the inelastic collision reaction cross section in the 100–250-MeV energy region [1]. Typically, the p–Si interaction has a reaction cross section of 400 mb in this energy region. In the resonance, the π–Si interaction can reach up to 800 mb.

Pions differ from protons and neutrons because they are lighter (rest mass 139.47 MeV/c^2) and they can have positive, negative, or neutral charge. The inelastic collision mechanism is dominant when it comes to SEE generation. However, negative pions can also be absorbed by the nucleus. The consequent deexcitation leads to secondary emission of particles capable of causing SEEs. Different from protons and neutrons, charged pions decay into muons or electrons within a few nanoseconds. Neutral pions decay even faster, making their flux completely negligible.

With such a short lifespan, pions can provide an important contribution to the SER only if electronic devices are located nearby pion generation points. This is the case of particle accelerators where electronics is subject to pion fluxes in amounts comparable to those of protons and neutrons [2], [3]. Pions can also be found in the atmospheric environments since they are part of the cosmic ray cascade, which is responsible for the formation of high neutron and muon fluxes. Most of the muons in the atmosphere are generated by the decay of pions. The pion fluxes in the atmosphere are more important at higher altitudes [4], but these fluxes are still a few orders of magnitude lower than those of neutrons.

Even when pion fluxes are important, the standard radiation hardness assurance (RHA) approach is to assume that pion SEE cross sections are identical to those of protons and neutrons at energies above 20 MeV. For this reason, the 200-MeV proton data point is commonly used to predict the mixed-field SER in the accelerator [5]. Not many experimental radiation data for pion-induced SEE exist in the literature, and none of such experiments was performed within the last 15 years, despite the emerging challenges introduced by recent deep submicrometer technologies. The existing radiation data are also rather contrasting. A first work on dynamic random access memories (DRAMs) single-event upsets (SEUs) [6] pointed out a quite predominant increase in the pion SEU cross section when compared to that of protons. Depending on the technology employed by the different manufacturers, the pion cross section was found to be as high as three times that of protons. A second work on static random access memories (SRAMs) and DRAMs' SEUs [7], though showing that the reaction cross-section resonance is somewhat reflected in an increase in the SER, still shows that this increase is much less pronounced. Thus, no conclusion concerning a pion enhancement of the SER was confirmed.

This article aims at extending the knowledge about the pion reaction resonance and its possible effects on the SER in the mixed field. Experimental data collected at the Paul Scherrer Institute (PSI) with monoenergetic pion beams show that the pion SEE cross section of commercial SRAMs is typically higher than the proton SEE cross sections at energies above 75 MeV. The experimental investigation dealt not only with SEUs but also with single-event latchups (SELs). The pion reaction resonance was investigated through FLUKA2011

Manuscript received November 28, 2019; revised January 27, 2020 and February 9, 2020; accepted February 29, 2020. Date of publication March 4, 2020; date of current version July 16, 2020. This work was supported by the European Union's Horizon 2020 Research and Innovation Programme through the Marie Sklodowska-Curie (MSC) under Grant 721624.

Andrea Coronetti, Rubén García Alía, and Matteo Cecchetto are with CERN, 1211 Geneva, Switzerland (e-mail: andrea.coronetti@cern.ch).

Wojtek Hajdas is with the Paul Scherrer Institute, Forschungsstrasse 111, 5232 Villigen, Switzerland.

Daniel Söderström and Arto Javanainen are with the Jyväskylän Yliopisto, 40500 Jyväskylä, Finland.

Frédéric Saigné is with the Institut d'Électroniqe et des Systèmes, Université de Montpellier, 34090 Montpellier, France.

Color versions of one or more of the figures in this article are available online at http://ieeexplore.ieee.org.

Digital Object Identifier 10.1109/TNS.2020.2978228

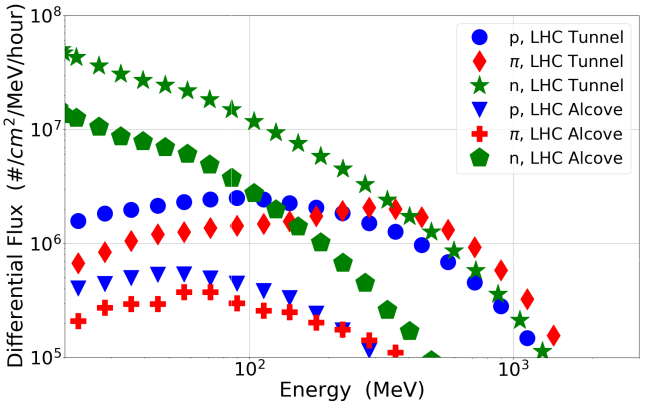

Fig. 1. Pion, proton, and neutron differential fluxes in typical accelerator mixed-field environment for two CHARM configurations representative of the LHC tunnel and the shielded alcoves [11].

2x.6 Mar 19 [8] simulations to understand why pions have a higher probability of inducing SEEs over the wide range of technological processes under analysis. The fundamental implications for RHA SER predictions of accelerator electronics are reasserted to account for this effect. The impact on the high-energy hadron (HEH) equivalence [3] for mixed-field SER predictions is also reassessed.

II. High-Energy Accelerator Environment

Along with protons and neutrons, pions are an important contributor to the overall mixed-field environment typical of the CERN accelerator complex. They are released over a widespread energy spectrum by the high-energy spallation reactions (production threshold energy = 141 MeV [9]) of the primary proton beam at the interaction points in p–p collisions [10] but also in collisions with beam intercepting devices (e.g., collimators) and with the residual gas in the vacuum pipes.

Fig. 1 shows a comparison of the pion, proton, and neutron differential energy spectra for a typical CERN Highly AcceleRated Mixed-field facility (CHARM) [12] configuration representative of the large hadron collider (LHC) tunnel and the shielded alcoves. The graph shows that the differential pion flux is similar to the proton flux. However, the peak pion flux is located between 300 MeV and 1 GeV, i.e., above the resonance region.

Table I reports on the hadronic abundance of each type of hadron and only accounts for energies above 20 MeV. This is the minimum energy that charged pions and protons must have to overcome the Coulomb barrier (when considering also their energy loss through standard microelectronic packaging structures). When it comes to SEEs, neutrons tend to dominate most of the accelerator relevant environments. However, in R13, the pion abundance is very similar to that of neutrons. This position is used for the qualification of equipment to be located in very energetic radiative environments at CERN.

Traditionally, electronic systems used at CERN are qualified at CHARM because of its environment representativeness. Component qualification is alternatively performed using monoenergetic proton beams or neutron spallation sources. While the latter is quite similar to the CHARM qualification approach, monoenergetic proton testing covers only a small part of the actual spectrum. These monoenergetic data are then used to account also for the pion flux, under the assumption that the pion SEE cross section can be considered equivalent to that of protons.

TABLE I

Hadronic Abundance of HEHs ($E > 20$ MeV) for Some Test Positions Inside CHARM [11]. All Charged Pions Are Grouped Together

Position	Pions	Protons	Neutrons	Kaons
R5	15.7%	13.8%	69.9%	0.6%
R10	22.7%	17.3%	58.9%	1.1%
R13	37.0%	20.2%	42.8%	0.0%

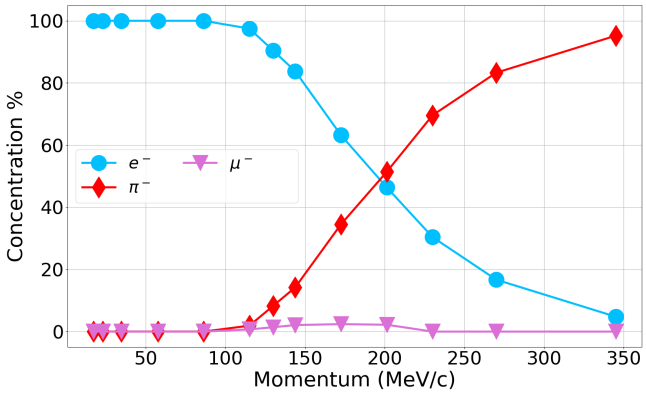

Fig. 2. Concentration of electrons, pions, and muons for negative polarity in percentage as a function of the momentum. Measurements performed with time-of-flight measurements [15].

III. Experimental Investigation

The experimental investigation focuses on SRAMs since these memories are widely used for the detection of radiation levels in the CERN LHC accelerator complex [13], as well as, in actual accelerator equipment designs exposed to radiation [14]. Since SRAMs are used to determine the HEH fluence in the mixed field, a direct assessment of their response to monoenergetic pions and protons was the best option.

A. Facilities

The PSI offers a wide range of particle beams for radiation to electronics effects' studies. Pions are produced at the piM1 facility [15] by the nuclear spallation of a 590-MeV proton monoenergetic beam from the high-intensity proton accelerator on a target. The secondary particles that are transported at the test position are pions, electrons, and muons. Pions can be found only with a momentum ranging from 115 to 345 MeV/c. However, the beam is not fully composed of pions, but its composition changes with the momentum. Fig. 2 shows the time-of-flight measurements performed by the facility to determine the beam composition at various momenta. Data were also extracted for the used momenta (130, 200, 270, and 345 MeV/c), which correspond, respectively, to 51, 104, 164, and 233 MeV in terms of pion energy.

The particles momentum is selected by a double bending magnet structure. The dosimetry instruments cannot differentiate among particles, and therefore, the beam compositions reported in Fig. 2 have to be accounted for when considering the actual flux of pions at the device under test (DUT). The maximum pion flux that can be extracted is 3×10^6 $\pi^-/\text{cm}^2/\text{s}$ at 233 MeV, but it gets as low as 5×10^4 $\pi^-/\text{cm}^2/\text{s}$ at 51 MeV.

Even for such cases when the beam is mostly composed of electrons (90% at 51 MeV), it is assumed that all the recorded events are induced by pions since electrons have SEU and SEL cross sections, which are at least three orders of magnitude lower [16].

Given the wide flux range, it was not possible to perform flux measurements at the facility using a single set of instruments. Three different methods were employed for pion flux logging. A first method, used for high energy (>100 MeV) and high flux ($>5\times10^5$ $\pi^-/\text{cm}^2/\text{s}$), made use of an ionization chamber positioned at the beam exit just before the DUT. A second method, used for lower energy beams (51 MeV only), made use of the proton current measurements upstream the spallation target which were converted into a pion flux by calibration with a scintillator. A final method, employed for high-energy beams (>100 MeV) and low flux ($<5\times10^5$ $\pi^-/\text{cm}^2/\text{s}$), consisted in measuring the beam intensity from the current produced by a scintillator. This was first located in place of the DUT for calibration means and then positioned behind the DUT during the tests.

Considering the uncertainties on the beam composition measurements and the use of various sets of instruments to retrieve the flux, a global uncertainty of ±20% on the beam fluence is accounted for the cross-sectional error bars. The spatial homogeneity of the beam (±10%) was attained only for a spot size with 10 mm diameter and was measured using a pixelated ionization chamber.

Proton testing has been performed at the Kernfysisch Versneller Instituut (KVI-CART facility) and the proton irradiation facility (PIF) in PSI. For KVI-CART, the same cyclotron can be tuned to provide protons with a primary energy of 190 or 66.5 MeV. The PIF cyclotron can accelerate proton up to a primary energy of 230 MeV. At both cyclotrons, the primary energies were also degraded into lower and intermediate energies (30–164 MeV) using aluminum or copper slabs of several thicknesses. For proton irradiation, the experiments were conducted using fluxes in the order of 10^7 $\text{p/cm}^2/\text{s}$ for SEU and $3\times10^5-10^6$ $\text{p/cm}^2/\text{s}$ for SEL. In both facilities, the beam is homogeneous within ±10% over a large area (5–10 cm^2). The beam intensity is monitored with ionization chambers and the fluence is determined within an uncertainty of ±10%.

B. Experimental Results

This study was performed by analyzing the SEE response of a set of six commercial complementary metal–oxide–semiconductor (CMOS) SRAMs with technological nodes varying from 250 to 40 nm. Four of these six memories were characterized against their SEU response, whereas the other two were known to have a relatively high SEL proton cross section that could be relevant for the limited pion flux available. The main data about these memories are reported in Table II. The first three SRAMs in Table II were irradiated lid-off, and the last three were irradiated lid-on. This is not expected to have a significant impact on the beam energy with these particles. The same date codes were irradiated with both protons and pions. In some cases, exactly, the same part was irradiated.

TABLE II
LIST OF TESTED DEVICES AND THEIR FEATURES

Reference	Array size, Mbits	Technology	Lid
AT86166H-YM20-E	4	250nm	off
CY62157EV30LL-45ZSXI	8	90nm	off
CY62167EV30LL-45ZXA	16	90nm	off
IS61WV204816BLL	32	40nm	on
BS62LV1600EIP55	16	180nm	on
LY62W20488ML	16	180nm	on

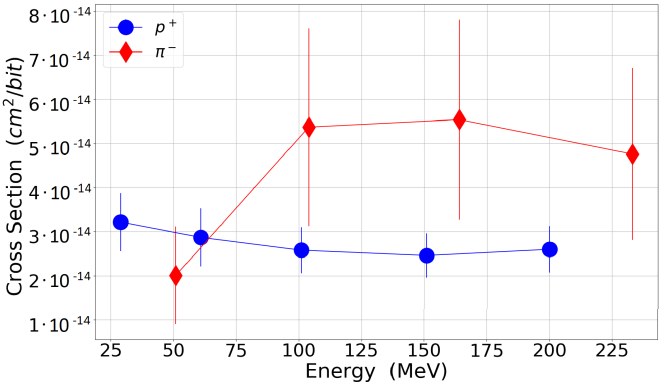

Fig. 3. Pion and proton SEU cross section for the Atmel SRAM with 95% confidence level error bars.

The same test logic was applied to both pion and proton irradiations. For SEU measurements, the SRAMs were programmed with a checkerboard pattern and a fixed fluence of 10^{10} π^-/cm^2 (p/cm^2) was targeted. This was sufficient to accumulate a statistically valuable amount of upsets. For SEL measurements, the test was stopped once at least 100 events had been observed. Tests were performed only at room temperature and within the datasheet nominal voltage. The current threshold was set to 10 mA with a hold time of 0.6 s and a reset time of 0.9 s.

All SRAMs have been irradiated under negative pions at four energies ranging from 51 to 233 MeV. For protons, four to six energies were selected in the 30–200-MeV range.

A direct comparison of proton and pion SEU cross sections is available in Figs. 3–6 for each of the commercial references previously listed. No matter the actual sensitivity of the single part, the technological process or the fact that they were lid-on or lid-off, all the data point out that the pion cross section at energies above 75 MeV is about a factor of 1.5–2.5 higher than its proton counterpart. Some of the measurements were repeated during a second run and their outcomes were very consistent with the first round of measurements. This seems to indicate that the uncertainty on the fluence is lower than what was shown by the error bars for the pion data.

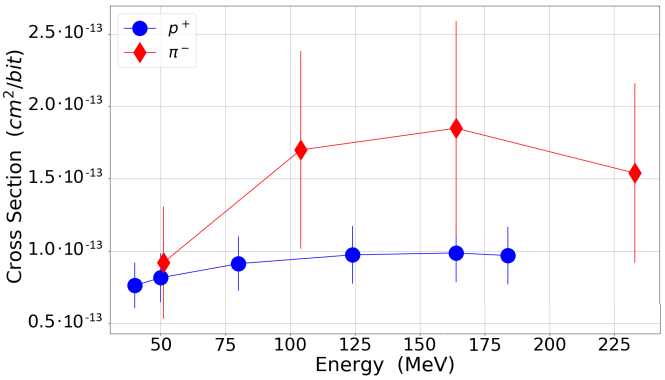

Fig. 4. Pion and proton SEU cross section for the cypress-45ZSXI SRAM with 95% confidence level error bars.

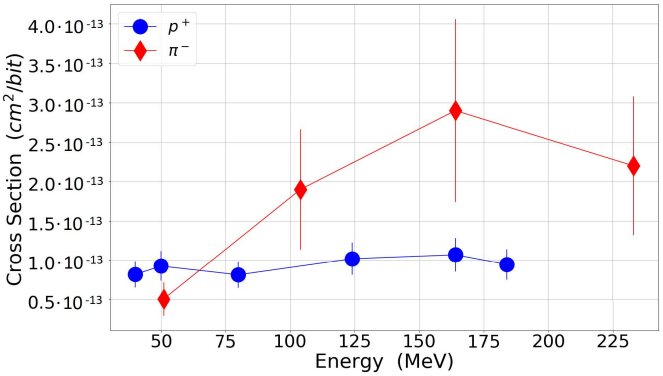

Fig. 5. Pion and proton SEU cross section for the cypress-45ZXA SRAM with 95% confidence level error bars.

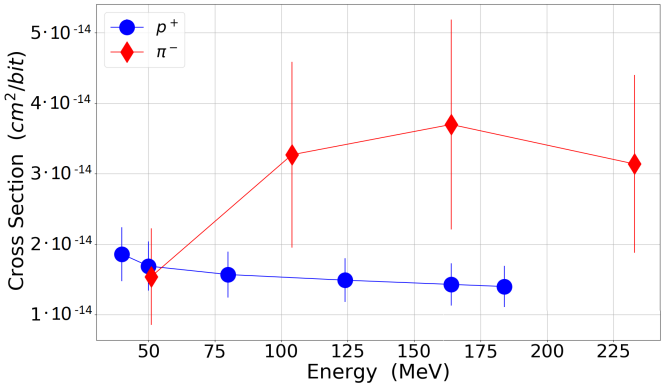

Fig. 6. Pion and proton SEU cross section for the ISSI SRAM with 95% confidence level error bars.

Concerning SEL measurements, data are compared in Figs. 7 and 8. The data seem to confirm the same trend that was observed with SEU for energies above 75 MeV. However, in the SEL case, the cross section does not drop so sharply and it is still higher than that of proton at 51 MeV for both SRAMs by a factor 2 and 3.

IV. Simulations of Pion SEU Cross Sections

The numerical data are retrieved through FLUKA-based Monte Carlo simulations. The basis of the simulations stands in finding suitable parameters for the sensitive volume (SV)

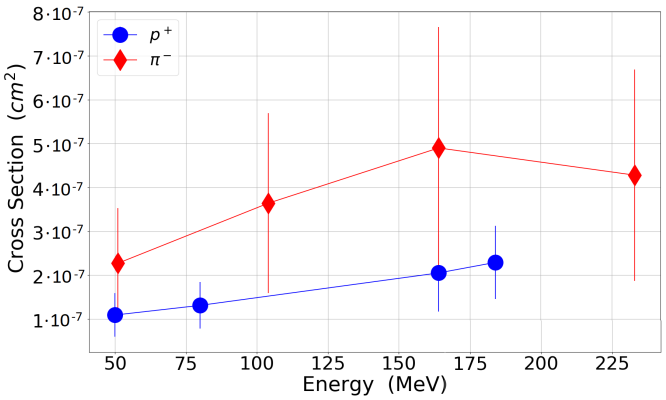

Fig. 7. Pion and proton SEL cross section for the brilliance SRAM with 95% confidence level error bars.

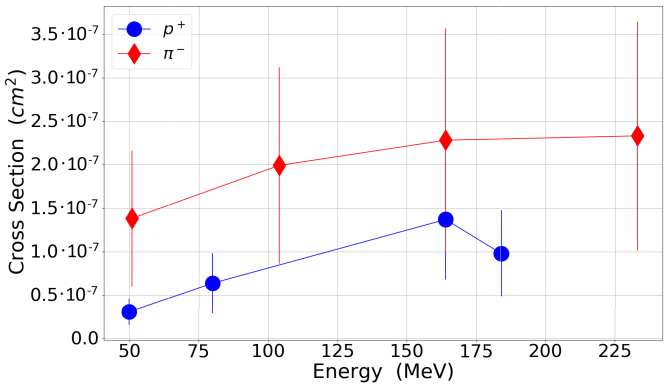

Fig. 8. Pion and proton SEL cross section for the Lyontek SRAM with 95% confidence level error bars.

model that would provide energy deposition events probability whose fitting matches the proton experimental cross section at 184 MeV. The 184-MeV proton point is chosen because it is used for the HEH approximation in mixed field, and for SEU, it is a good reference for the saturation cross section. The attained rectangular parallelepiped (RPP) model size and critical charge are then implemented for the simulations with all other hadrons: charged pions, neutrons, and charged kaons.

The analysis focuses on the Integrated Silicon Solution Inc. (ISSI) SRAM, which is a state-of-the-art technology. Its radiation response and RPP modeling were benchmarked in [17]. A critical charge of $\approx$0.75 fC was found to be suitable in describing direct ionization phenomena from low-energy protons, and it is retained for this article. That article also proposed an SV size of 250 nm for the 40-nm technological node. A back end of line (BEOL) SiO_2 layer 6 μm thick is also added on top of the SV.

In this article, the SV size is taken as the free parameter of the cubic RPP for the high-energy proton data fitting. A side of 310 nm was chosen since it better approximates the 184-MeV proton experimental point, 1.4×10^{-14} cm^2/bit, whereas the 250-nm returned a cross section of 0.9×10^{-14} cm^2/bit. A larger volume better accounts from more spread drift and diffusion collection mechanisms from higher energies. A validation of the proposed model is reported in Fig. 9. The figure shows that both proton and pion experimental cross sections are well reproduced

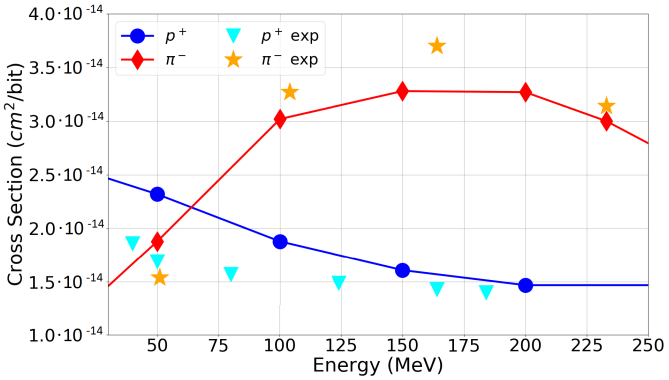

Fig. 9. Simulated cross sections for protons and negative pions and comparison with experimental data for the ISSI memory.

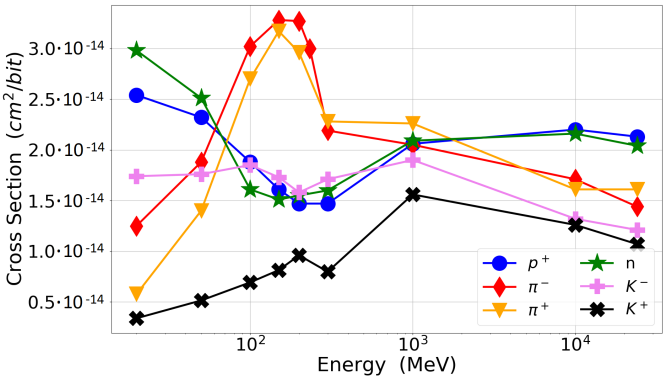

Fig. 10. Simulated cross sections for protons, charged pions, neutrons, and charged kaons over typical CHARM energy distributions for an RPP with 310-nm side and 0.75-fC critical charge.

within a worst case factor 2 for protons at 50 MeV. Discrepancies at this energy are likely due to the presence of the plastic packaging as well as the absence of a detailed BEOL material description. The numerical pion SEU cross sections are calculated within an error of 25% at 100 MeV and 45% at 50 MeV.

The model was run for six particles and nine energies each to cover the 20 MeV–24-GeV energy interval typical of the CHARM mixed field. The data are shown in Fig. 10. According to the simulations, the pion SEU resonance is restricted to the 75–250-MeV region. The resonance peak well reproduces the factor 2 increase, which was experimentally observed.

The pion SEU experimental decrease below 100 MeV is also reproduced by the strong lowering of the simulated pion cross section at 20 and 50 MeV if compared to the enhanced proton and neutron cross sections. However, the 50-MeV pion point has the same magnitude as the 200-MeV proton point. After the numerical results, this simple RPP seems capable of grasping all of the nuclear mechanisms affecting the pion SEU cross section. The use of a nested RPP model [18] did not provide significant differences.

The proposed RPP model with 0.75-fC critical charge and 310-nm size is retained for the later RHA implications since it very well describes the resonance.

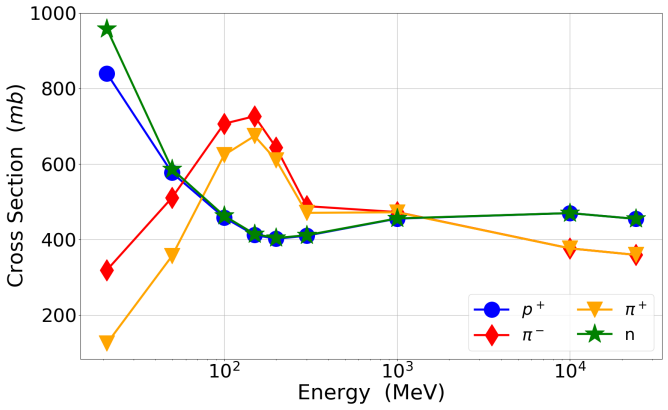

Fig. 11. Reaction cross section in silicon of protons, pions, and neutrons showing a resonance in the 100–250-MeV energy region (obtained from FLUKA).

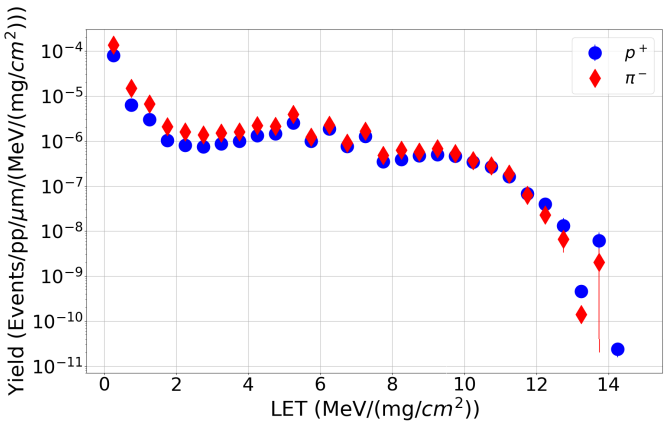

Fig. 12. Yield of secondary ions produced by nuclear reactions as a function of their LET for negative pions and protons at 200 MeV.

V. Nuclear Interaction Mechanisms

The observed pion SEE cross-section resonance is the reflection of the nuclear inelastic cross section (see Fig. 11) for these particles. This figure shows that within the concerned energy range, pions have a much higher probability of interacting with the Si nuclei than the other hadrons do.

The characteristics of the secondary ions from π-Si collisions are responsible for the SEU cross section behavior too. Such quantities were scored in FLUKA upon production to quantify the differences between protons and negative pions' secondary recoils. Fig. 12 shows a quantification of the event probabilities per incident particles for various linear energy transfer (LET) intervals at 200 MeV. Pions are twice as effective as protons in generating low LET [$<$5 MeV/(mg/cm^2)] secondary ions and up to 50% more effective for intermediate LET [$<$10 MeV/(mg/cm^2)] secondary ions. Similarly, there is an excess of low Z recoils for pions if compared to protons (see Fig. 13). A similar higher fragmentation mechanism with more low LET secondary ions is responsible for the proton and neutron SEU cross-sectional enhancements above 1 GeV.

On the contrary, pion nuclear interactions release a smaller amount of high-Z (and high LET) recoils than protons. At 200 MeV, this yield is not that effective in limiting the

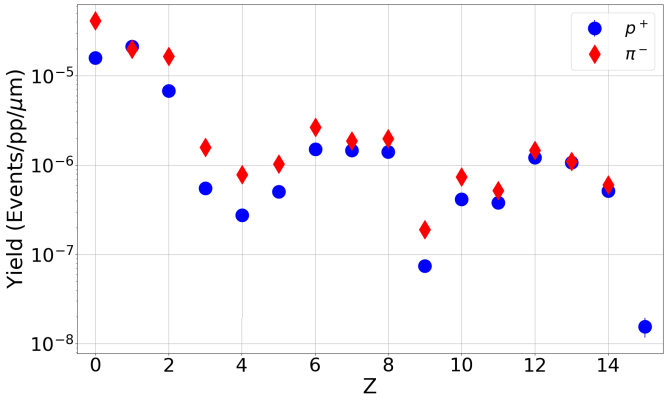

Fig. 13. Yield of secondary ions produced by nuclear reactions as a function of their atomic number for negative pions and protons at 200 MeV.

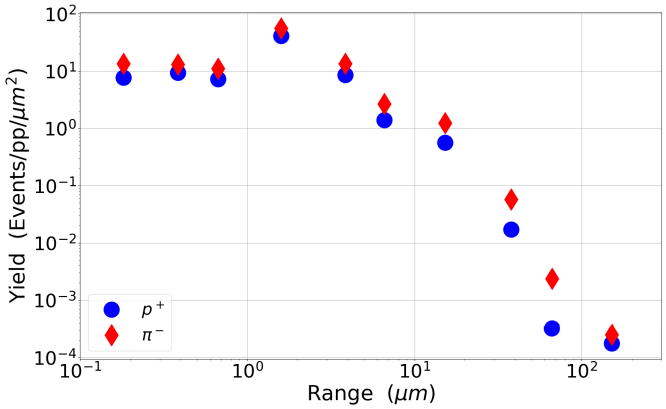

Fig. 14. Yield of secondary ions produced by nuclear reactions as a function of their range for negative pions and protons at 200 MeV.

pion SEU resonance. Fig. 14 also reports on the range of secondary ions having an LET $>$ 1 MeV/(mg/cm^2), which confirms that pion recoils are usually associated with a longer range than proton recoils.

Fig. 15 shows the event probability distribution as a function of LET when the energy of the incident particles is reduced to 50 MeV. The pion yield is very similar to that of protons for low LET secondary ions but becomes $>$50% lower for intermediate and high LET secondary ions. This is further stressed by the comparison of LET distributions of the Si recoils, as shown in Fig. 16. Pions are ineffective in producing these recoils at intermediate and high LET since the kinetic energy content that is imparted to the Si ions is below 100 keV/n. As a result, Si recoils from π–Si interactions above 6 MeV/(mg/cm^2) have negligible probability of being created when compared to the same recoils released by p–Si interaction, which have high production probability up to an LET as high as 12 MeV/(mg/cm^2). Fig. 17 also shows the ranges of the secondary recoils with LET $>$ 1 MeV/(mg/cm^2) at 50 MeV. This figure also shows that even though protons produce a larger number of short-ranged recoils, pions can still produce recoils with quite extended range.

The excess in low and intermediate LET recoils from $>$100-MeV pions is thus justified by higher π-Si interaction

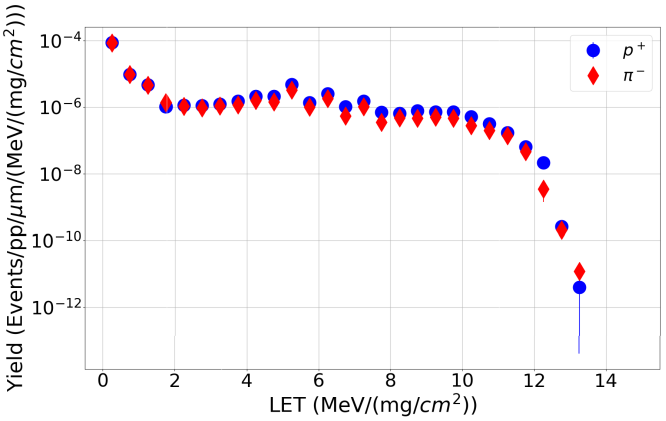

Fig. 15. Yield of secondary ions produced by nuclear reactions as a function of their LET for negative pions and protons at 50 MeV.

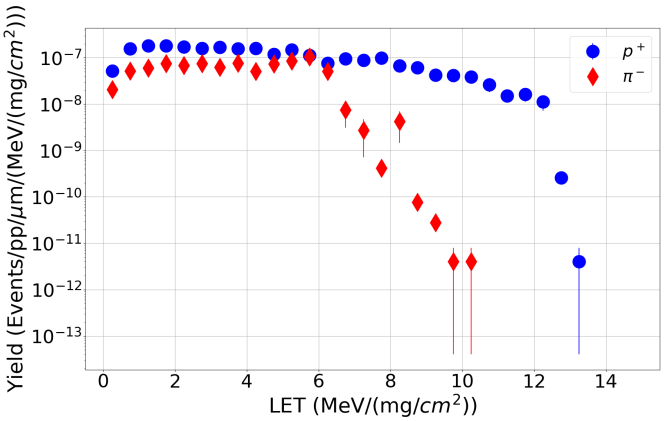

Fig. 16. Yield of secondary ions produced by nuclear reactions as a function of their LET for Si recoils for negative pions and protons at 50 MeV.

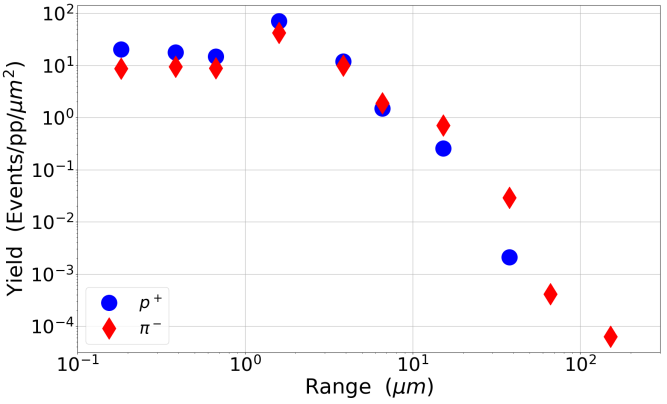

Fig. 17. Yield of secondary ions produced by nuclear reactions as a function of their range for negative pions and protons at 50 MeV.

probability and by larger fragmentation of the silicon nuclei. This may also explain why, in previous studies based on older technologies [7], the pion resonance was sometimes not observed. If the heavy-ion LET threshold of the device is indeed higher than 6 MeV/(mg/cm^2), then the enhanced production of low LET secondary ions will not contribute to an increase in the SEU cross section.

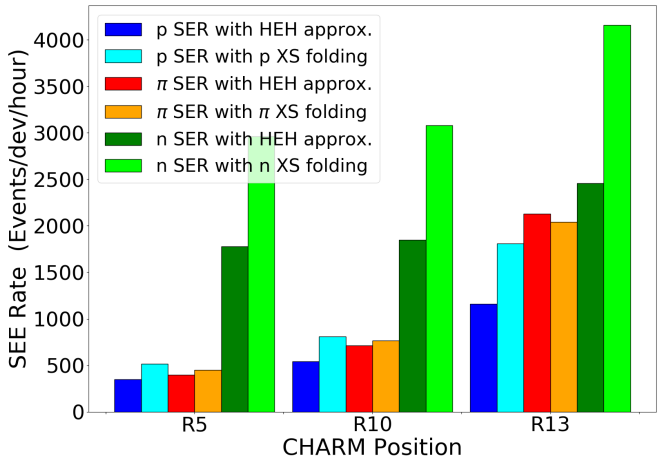

Fig. 18. SER comparison between the HEH approximation approach and the full particle folding approach. Data are reported by the CHARM position and further subdivided for protons (blue), pions (red), and neutrons (green).

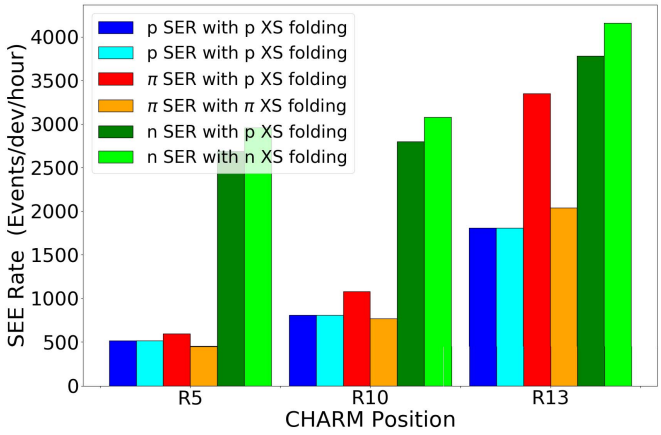

Fig. 19. SER comparison between the proton only folding approach and the full particle folding approach. Data are reported by the CHARM position and further subdivided for protons (blue), pions (red), and neutrons (green).

VI. RHA Implications

The CHARM mixed field is certainly a valuable mean to assert RHA practices devoted to the accelerator equipment qualification. The many different positions with respect to the target in the irradiation room allow maintaining the representativeness of many radiative environments within the CERN accelerator complex, but they can also be extended to various electronic equipment tests for other environments, e.g., space. In this context, the interest is to assess if the pion SEU resonance can affect the radiation response when compared to a standardized qualification made with monoenergetic protons [19].

The actual HEH SEU cross section is a single value determined by the contribution of a wide energetic multiparticle spectrum. The HEH approximation claims that this HEH SEU cross section can be assumed to be equivalent to the 200-MeV proton SEU cross section. The approximation stands in assuming that all the particles' responses are identical, no matter the particle types and their energy above 20 MeV.

The nuclear interaction analysis and simulations performed for the ISSI SRAM allows implementing a set of comparison to determine the SER of this specific device based on the simulated cross sections. Fluxes from each particle inside the CHARM irradiation room are scored by simulating the model of the facility. The SER can be obtained according to the following approaches:

1) by the integral of all particle fluxes above 20 MeV multiplied by the 200-MeV proton cross section (HEH approximation);
2) by folding all particle fluxes above 20 MeV with the proton cross-sectional curve as a function of energy (approach typical of standards [19]);
3) by folding each particle flux above 20 MeV with its own particle cross section (the actual HEH cross section with no approximation other than using simulation data and excluding the neutron contribution below 20 MeV).

Fig. 18 shows a first comparison between the first and the third SER calculation philosophies. This first comparison allows drawing conclusions about the suitability of using monoenergetic proton facilities for testing electronic equipment to be installed in the accelerator. The comparison is made for three significant positions inside CHARM (R5: low-Earth orbit (LEO) space-like spectra, R10: accelerator and atmospheric-like spectra, and R13: accelerator-like spectra for very energetic environments) and on a particle-by-particle basis. The graph shows that no matter which approach is pursued, neutrons will dominate the SER response in positions R5 and R10 and they stand out as the main contributor for position R13 too.

The pion response is the one that is less affected by the HEH approximation. The differences between protons and neutrons are higher. This is due to their increased cross section between 20 and 100 MeV, shown in Fig. 10, compared to their 200-MeV value which is taken as energy reference for the HEH approximation. The SER of pions from the HEH approximation is underestimated by just 10%, whereas those for protons and neutron by 33% and 42%, respectively. When all contributions are summed up, the HEH approximation is underestimating the SER by 33% in R5 and by 28% in R13.

A similar comparison between the folding of the proton cross section (second approach) and the folding of all the cross sections (third approach) yields very similar SERs (Fig. 19). In this case, the folding of the proton cross section may lead to slight overestimations of the SER. Pions are also the particles whose SER differs the most. This is mainly due to the 20–50-MeV proton cross section being higher than the 20–50-MeV pion cross section in an energy region where pion fluxes are not negligible. The differences resulting from this comparison is a 3% underestimation for R5 and a 10% overestimation for R13.

To conclude, the pion SEU resonance is seen not to be the main factor affecting the cross-sectional estimations in a mixed-field environment because, first, the SER is dominated by neutrons (in the 20–100-MeV range, in particular) and, second, because the peak pion flux does not correspond to the resonance region. Testing an electronic device to be used in the accelerator at a monoenergetic proton facility with 200 MeV protons (first approach) brings to an accelerator SER

TABLE III
COMPARISON BETWEEN APPROACHES 2 AND 3 FOR LEO SER PREDICTIONS

	SER proton test	**SER CHARM**	**Ratio**
Orbit	(events/dev/hour)	(events/dev/hour)	
400 km, 98°, Solar min	$2.80 \cdot 10^{-2}$	$2.57 \cdot 10^{-2}$	1.09
400 km, 51°, Solar min	$4.21 \cdot 10^{-2}$	$3.84 \cdot 10^{-2}$	1.10
800 km, 98°, Solar min	$3.62 \cdot 10^{-1}$	$3.35 \cdot 10^{-1}$	1.08
800 km, 51°, Solar min	$5.35 \cdot 10^{-1}$	$4.92 \cdot 10^{-1}$	1.09

underestimation of up to 33%, which is still quite satisfactory. Performing standard proton cross-sectional measurements at multiple energies and folding the cross section with the actual mixed-field fluxes (second approach) would lead to an even better fit. This shows that there is no particular information lost if pion and neutron responses are unknown. Fitting of experimental data is expected to be even better since there is no experimental evidence of such a strong increase in the proton and neutron cross sections at 20–100 MeV.

Another analysis can be done to study which is the level of approximation introduced by testing a device in a mixed field for a different environment than the accelerator, e.g., space. Still using simulation data, the actual HEH SEU cross section that would be retrieved from a CHARM experiment for the ISSI SRAM is 2.29×10^{-14} cm^2/bit. Multiplying this cross section for some typical space fluxes (above 20 MeV and obtained from OMERE [20]) would lead to proton-induced SERs that are underestimated by 10% or less (see Table III).

VII. CONCLUSION

Measurements of pion SER have been often overlooked, assuming that their cross section would match that of protons and neutrons. Pions are, nonetheless, a central contributor to the SEE response in accelerators. Their cross section was experimentally observed to differ from that of protons for both SEU and SEL in the energy region between 50 and 230 MeV.

The proposed numerical model confirmed that the SEU response of pions strictly reflects the inelastic cross section of π–Si collisions. The increased SEU cross section in the 75–250-MeV region was seen to be related to an enhancement in the production of low and intermediate LET secondary ions. The <75-MeV drop in the pion SEU cross section is also justified by the less effective production of intermediate and high LET secondary ions at these lower incident energies.

The impact of the pion SEU resonance in a mixed-field environment was assessed for the sake of RHA practices. The resonant pion SEE cross section was found not to affect the radiation response of a device in the mixed field. Due to their higher fluxes, neutrons remain the dominating contributor to the SEE global response.

Both the HEH approximation (200-MeV proton testing only) and the proton cross-sectional folding approaches were shown to be reliable techniques for the SER prediction of electronic devices to be used in the accelerator environment. At the same time, the mixed-field response was demonstrated to be similar to that of a radiative field mainly composed of protons, proving the suitability of using CHARM for qualification of electronics to be used in proton- or neutron-dominated environments.

REFERENCES

[1] H. H. K. Tang, "Nuclear physics of cosmic ray interaction with semiconductor materials: Particle-induced soft errors from a physicist's perspective," *IBM J. Res. Develop.*, vol. 40, no. 1, pp. 91–108, Jan. 1996.

[2] R. Garcia Alia *et al.*, "LHC and HL-LHC: Present and future radiation environment in the high-luminosity collision points and RHA implications," *IEEE Trans. Nucl. Sci.*, vol. 65, no. 1, pp. 448–456, Jan. 2018.

[3] K. Roeed *et al.*, "Method for measuring mixed field radiation levels relevant for SEEs at the LHC," *IEEE Trans. Nucl. Sci.*, vol. 59, no. 4, pp. 1040–1047, Aug. 2012.

[4] J. Barak and N. M. Yitzhak, "SEU rate in avionics: From sea level to high altitudes," *IEEE Trans. Nucl. Sci.*, vol. 62, no. 6, pp. 3369–3380, Dec. 2015.

[5] R. G. Alía *et al.*, "Single event effects in high-energy accelerators," *Semicond. Sci. Technol.*, vol. 32, no. 3, 2017, Art. no. 034003.

[6] G. J. Hofman *et al.*, "Light-hadron induced SER and scaling relations for 16- and 64-mb DRAMS," *IEEE Trans. Nucl. Sci.*, vol. 47, no. 2, pp. 403–407, Apr. 2000.

[7] S. Duzellier, D. Falguere, M. Tverskoy, E. Ivanov, R. Dufayel, and M.-C. Calvet, "SEU induced by pions in memories from different generations," *IEEE Trans. Nucl. Sci.*, vol. 48, no. 6, pp. 1960–1965, Dec. 2001.

[8] *FLUKA*. Accessed: Feb. 2020. [Online]. Available: http://fluka.cern

[9] J. Mårtensson *et al.*, "Pion production excitation functions in proton-nucleus collisions from the absolute threshold to 500 MeV," *Phys. Rev. C*, vol. 62, Jun. 2000, Art. no. 014610.

[10] S. J. Bates *et al.*, "Pion-induced damage in silicon detectors," *Nucl. Instrum. Methods Phys. Res. A, Accel., Spectrometers, Detectors Associated Equip.*, vol. 379, no. 1, pp. 116–123, Sep. 1996.

[11] A. Infantino, "FLUKA Monte Carlo modelling of the CHARM facility's test area: Update of the radiation field assessment," CERN, Geneva, Switzerland, Tech. Rep. CERN-ACC-NOTE-2017-0059, Nov. 2017.

[12] J. Mekki, M. Brugger, R. G. Alia, A. Thornton, N. C. Dos Santos Mota, and S. Danzeca, "CHARM: A mixed field facility at CERN for radiation tests in ground, atmospheric, space and accelerator representative environments," *IEEE Trans. Nucl. Sci.*, vol. 63, no. 4, pp. 2106–2114, Aug. 2016.

[13] G. Spiezia *et al.*, "A new RadMon version for the LHC and its injection lines," *IEEE Trans. Nucl. Sci.*, vol. 61, no. 6, pp. 3424–3431, Dec. 2014.

[14] S. Danzeca *et al.*, "Qualification and characterization of SRAM memories used as radiation sensors in the LHC," *IEEE Trans. Nucl. Sci.*, vol. 61, no. 6, pp. 3458–3465, Dec. 2014.

[15] W. Hajdas *et al.*, "High energy electron radiation exposure facility at PSI," *J. Appl. Math. Phys.*, vol. 2, no. 9, pp. 910–917, Aug. 2014.

[16] M. Tali *et al.*, "High-energy electron-induced SEUs and Jovian environment impact," *IEEE Trans. Nucl. Sci.*, vol. 64, no. 8, pp. 2016–2022, Aug. 2017.

[17] R. G. Alía, M. Tali, M. Cecchetto, F. Cerutti, and A. Cononetti, "Direct ionization impact on accelerator mixed-field soft-error rate," *IEEE Trans. Nucl. Sci.*, vol. 67, no. 1, pp. 345–352, Jan. 2020.

[18] B. D. Sierawski *et al.*, "Impact of low-energy proton induced upsets on test methods and rate predictions," *IEEE Trans. Nucl. Sci.*, vol. 56, no. 6, pp. 3085–3092, Dec. 2009.

[19] *Single Event Effects Test Method and Guidelines*, ESA ESTEC, Noordwijk, The Netherlands, Oct. 2014.

[20] *OMERE*. Accessed: Aug. 2019. [Online]. Available: http://www.trad.fr/spatial/logiciel-omere